Accepted Manuscript

Recovering an unknown source in a fractional diffusion problem

William Rundell, Zhidong Zhang
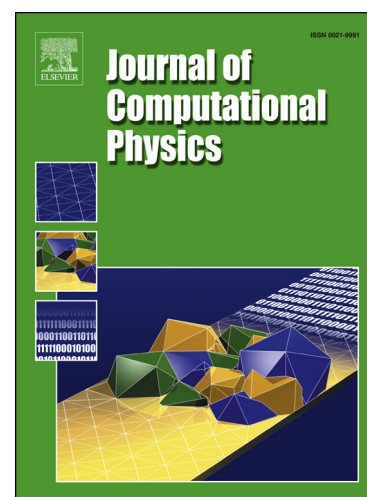
Please cite this article in press as: W. Rundell, Z. Zhang, Recovering an unknown source in a fractional diffusion problem, *J. Comput. Phys.* (2018), https://doi.org/10.1016/j.jcp.2018.04.046

Recovering an Unknown Source in a Fractional Diffusion Problem

William Rundell[*1] and Zhidong Zhang [†2]

[1]Department of Mathematics, Texas A&M University, USA
[2]Department of Mathematics and Statistics, University of Helsinki, Finland

April 30, 2018

Abstract

A standard inverse problem is to determine a source which is supported in an unknown domain D from external boundary measurements. Here we consider the case of a time-independent situation where the source is equal to unity in an unknown subdomain D of a larger given domain Ω and the boundary of D has the star-like shape, i.e.

$$\partial D = \{q(\theta)(\cos\theta, \sin\theta)^\top : \theta \in [0, 2\pi]\}.$$

Overposed measurements consist of time traces of the solution or its flux values on a set of discrete points on the boundary $\partial\Omega$. The case of a parabolic equation was considered in [6]. In our situation we extend this to cover the *subdiffusion* case based on an anomalous diffusion model and leading to a fractional order differential operator. We will show a uniqueness result and examine a reconstruction algorithm. One of the main motives for this work is to examine the dependence of the reconstructions on the parameter α, the exponent of the fractional operator which controls the degree of anomalous behaviour of the process. Some previous inverse problems based on fractional diffusion models have shown considerable differences between classical Brownian diffusion and the anomalous case.

Keywords: fractional diffusion equation, inverse problem, uniqueness, unknown discontinuous source, Newton's method, Tikhonov regularization.

AMS subject classifications: 35R11, 35R30, 65M32.

1 Introduction

Our aim is to recover the location and shape of an extended source function $F = \chi_D$ in a diffusion problem from making time-trace boundary measurements,

$$\begin{cases} {}^C D_t^\alpha u - \triangle u = \chi_D, & (x,t) \in \Omega \times [0,T]; \\ \quad u(x,0) = 0, & x \in \Omega; \\ \quad u(x,t) = 0, & (x,t) \in \partial\Omega \times [0,T]. \end{cases} \tag{1.1}$$

---

[*]rundell@math.tamu.edu
[†]zhidong.zhang@helsinki.fi

$\Omega \subseteq \mathbb{R}^2$ is the unit disc, χ_D is the characteristic function on D which is the source domain we need to recover with $\overline{D} \subseteq \Omega$. The overposed data is a time trace of the flux at a (small) finite number m of points located on the boundary $\partial \Omega$,

$$\frac{\partial u}{\partial \overrightarrow{\mathbf{n}}}(z_\ell, t) = g_\ell(t), \ t \in [0, T], \ \ell = 1, \ldots, m.$$

In this paper, we restrict the set of admissible boundaries to be star-like domains with respect to a point within Ω,

$$\partial D = \{q(\theta)(\cos\theta, \sin\theta)^\top : \theta \in [0, 2\pi]\}$$

with a smooth, periodic function $0 < q(\theta) < 1$. In equation (1.1) $^C D_t^\alpha$ denotes the Djrbashian-Caputo fractional derivative of order α, $0 < \alpha < 1$ which will be defined in the next section.

We have described (1.1) in the simplest setting in the sense we have taken the exterior boundary to be the unit circle and have chosen homogeneous initial and boundary data. This simplifies the exposition and, in particular, many of the representation formulae. Adding in nonhomogeneous initial/boundary conditions: $u(x, 0) = u_0(x)$ and $u(x, t) = f(x, t)$ for x on $\partial \Omega$ and sufficiently smooth f, would be completely straightforward. Taking Ω to be a simply connected domain with C^2 boundary $\partial \Omega$ is also possible in theory but we have used the specific eigenfunction expansion for $-\triangle$ for a circle in both the uniqueness result and the reconstruction algorithm. The key change would be to equations (3.5) and (3.10) where the trigonometric function would have to be replaced by the values of the Laplace eigenfunctions for Ω evaluated on $\partial \Omega$. While these share the same properties when Ω is the unit circle, this extension would require some further analysis.

The model (1.1) represents a so-called *anomalous diffusion* process generalizing classical, Brownian diffusion based on the heat equation. This latter model can be viewed as a random walk in which the dynamics are governed by an uncorrelated, Markovian, Gaussian stochastic process. The key assumption is that a change in the direction of motion of a particle is random and that the mean-squared displacement over many changes is proportional to time, i.e. $\langle x^2 \rangle = Ct$. This easily leads to the derivation of the underlying differential equation being the heat equation. On the other hand, when the random walk involves correlations, non-Gaussian statistics or a non-Markovian process (for example, due to "memory" effects) the classical diffusion equation will fail to describe the macroscopic limit. For example, if we replace the space-time correlation by $\langle x^2 \rangle = Ct^\alpha$ then it can be shown that this leads to a *subdiffusive* process and, importantly leads to a tractable model where the partial differential equation is replaced by the nonlocal equation (1.1).

This paper is a generalisation of [6] where the same problem was considered for the classical parabolic case, $\alpha = 1$. Our approach will be the same, but here we must deal with the technical issues of replacing the far simpler classical time derivative by the nonlocal operator $^C_a D_t^\alpha$. Thus while in the case $\alpha = 1$ (1.1) is pointwise defined and the Markovian property dictates that for any time step t the solution can be uniquely obtained from any single previous step $t - \delta t$, this is far from the case if $\alpha < 1$ where the complete time history of the function u has to be retained in the evolution. In some previous cases involving fractional derivatives the inverse problem has very different properties, especially with respect to degree of ill-conditioning, from the classical case. See [10] for an overview. The poster child here is the backward diffusion problem. This is severely ill-conditioned for the heat equation, but for $0 < \alpha < 1$ is only moderately so (equal to a 2-derivative loss) , [2]. Thus an important aspect of our studies here is to determine, if any, the differences made by the anomalous diffusion operator from that of the classical one. For some other works in this direction we refer to [13, 16] which use Bayesian formulation to study fractional inverse problems, and [9] which concerns an inverse Sturm-Liouville problem and [11] in which a strong maximum principle for fractional diffusion equations is deduced. We will also investigate the influence of the number m of measurement points on both the question of uniqueness and reconstruction.

2 Preliminary material

2.1 Fractional derivatives

The (left-sided) fractional integral of order α is defined for $f \in L^1(a,b)$ by

$$(_aI_x^\alpha f)(x) = \frac{1}{\Gamma(\alpha)} \int_a^x (x-s)^{\alpha-1} f(s) \, ds, \tag{2.1}$$

and leads naturally to a fractional derivative in one of two ways. The (left-sided) Riemann-Liouville fractional derivative of order $0 < \alpha < 1$, is defined by

$$_a^R D_t^\alpha f(t) := \frac{1}{\Gamma(1-\alpha)} \frac{d}{dt} \int_a^t (t-s)^{-\alpha} f(s) \, ds,$$

and the (left-sided) Djrbashian-Caputo fractional derivative of order α by

$$_a^C D_t^\alpha f(t) := \frac{1}{\Gamma(1-\alpha)} \int_a^t (t-s)^{-\alpha} f'(s) \, ds.$$

In both cases note the specific dependence on the endpoint a. Some references are [3, 4, 1, 14, 15].

The Djrbashian-Caputo derivative is more restrictive than the Riemann-Liouville since it requires the classical derivative to be absolutely integrable and we implicitly assume that this condition holds. Generally, the Riemann-Liouville and Djrbashian-Caputo derivatives are different, even when both derivatives are defined, and we only have to consider the constant function to see this. Nonetheless, as we must expect, they are closely related to each other and under the assumption that the function to which they are applied vanishes at the starting point they are equal. Thus in (1.1) as stated we could have equally replaced $_0^C D_t^\alpha$ by $_0^R D_t^\alpha$. However, in the face of a non-homogeneous initial condition the regularity of the solution of the direct problem for (1.1) would change.

2.2 Mittag-Leffler function

This function plays a central role in fractional diffusion equations. It is a two-parameter function defined as

$$E_{\alpha,\beta}(z) = \sum_{k=0}^\infty \frac{z^k}{\Gamma(k\alpha + \beta)}, \ z \in \mathbb{C}.$$

The Mittag-Leffler function generalizes the exponential function since $E_{1,1}(z) = e^z$ and as $\alpha \to 1$ the fractional diffusion process recovers classical diffusion as described by the heat equation. The following property will be used later. The proof can be found in standard references, for example, [14, Lemma 3.2].

Lemma 2.1. *For $\lambda > 0$, $\alpha > 0$ and $n \in \mathbb{N}^+$, we have*

$$\frac{d^n}{dt^n} E_{\alpha,1}(-\lambda t^\alpha) = -\lambda t^{\alpha-n} E_{\alpha,\alpha-n+1}(-\lambda t^\alpha), \ t > 0.$$

In particular, $\frac{d}{dt} E_{\alpha,1}(-\lambda t^\alpha) = -\lambda t^{\alpha-1} E_{\alpha,\alpha}(-\lambda t^\alpha), \ t > 0.$

3

2.3 The direct problem for equation (1.1)

For the unit disc Ω, denote the eigensystem of the Laplacian $-\triangle$ with the Dirichlet boundary condition by $\{(\lambda_n, \varphi_n(x)) : n \in \mathbb{N}^+\}$. Here, $\{\lambda_n : n \in \mathbb{N}^+\}$ is indexed by nondecreasing order and strictly positive, and $\{\varphi_n(x) : n \in \mathbb{N}^+\}$ constitutes an orthonormal basis in $L^2(\Omega)$. The polar representation of φ_n is

$$\varphi_n(r, \theta) = w_n J_m(\sqrt{\lambda_n} r) \cos(m\theta + \phi_n), \qquad (2.2)$$

where $m = m(n)$, the phase ϕ_n is either 0 or $\pi/2$ and w_n is the normalized weight factor. Here $J_m(z)$ is the first kind Bessel function with degree m.

With the above, [14] gives the following theorem for the direct problem of (1.1). Here $H^k(\Omega)$ are the usual Sobolev spaces.

Theorem 2.1. *There exists a unique weak solution $u \in L^2(0, T; H^2(\Omega) \cap H_0^1(\Omega))$ of (1.1) with the representation*

$$u(x, t) = \sum_{n=1}^{\infty} \left(\int_0^t \int_D \varphi_n(y)(t - \tau)^{\alpha-1} E_{\alpha,\alpha}(-\lambda_n(t - \tau)^\alpha) \, \mathrm{d}y \, \mathrm{d}\tau \right) \varphi_n(x) \qquad (2.3)$$

and the regularity estimate

$$\|u\|_{L^2(0,T;H^2(\Omega))} + \|{}^C D_t^\alpha u\|_{L^2(\Omega \times (0,T))} \le C(T, D),$$

where the notation $C(T, D)$ indicates the dependence on the final time T and the domain D.

Proof. This theorem is a specific case of [14, Theorem 2.2] based on the fact that the source term is independent of t. See a later paragraph about generalizing the situation in (1.1) to include an unknown time-dependent factor in the source term. $\qquad \square$

3 Main results

In this section we will prove the main theoretical result: under suitable restrictions, two observation points are sufficient to determine the internal domain D uniquely.

3.1 Harmonic basis

Let $\xi_m^{c,s}(r, \theta) = \frac{1}{\pi} r^m \{\cos m\theta, \sin m\theta : m \in \mathbb{N}\}$ denote the set of harmonic functions in Ω. With the given normalization it forms a complete orthonormal basis in $L^2(\partial\Omega)$. First, we show that this basis can be used to gain a convergent approximation to the flux data $\frac{\partial u}{\partial \overline{\mathbf{n}}}(z_\ell, t)$ for $z_\ell \in \partial\Omega$.

Define the smooth approximation $\psi_\ell^M \in C^\infty(\overline{\Omega})$ of the delta distribution at z_ℓ as

$$\psi_\ell^M(x) = \sum_{m=1}^{M} \xi_m^c(z_\ell) \xi_m^c(x) + \xi_m^s(z_\ell) \xi_m^s(x),$$

and let the set of functions $\{u_\ell^M\}$ be weak solutions of the fractional diffusion equations

$$\begin{cases} {}^C D_t^\alpha u_\ell^M - \triangle u_\ell^M = 0, & (x, t) \in \Omega \times (0, T); \\ u_\ell^M = 0, & (x, t) \in \partial\Omega \times (0, T); \\ u_\ell^M = -\psi_\ell^M, & (x, t) \in \Omega \times \{0\}. \end{cases}$$

It follows from [14] that we have the regularity results $u_\ell^M \in C((0, T]; H^2(\Omega) \cap H_0^1(\Omega))$, ${}^C D_t^\alpha u_\ell^M \in C((0, T]; L^2(\Omega))$.

4

Lemma 3.1. *Define*

$$w_\ell^M = u_\ell^M + \psi_\ell^M, \tag{3.1}$$

then $w_\ell^M \in C((0,T]; H^2(\Omega) \cap H_0^1(\Omega))$, ${}^C D_t^\alpha w_\ell^M \in C((0,T]; L^2(\Omega))$ *and*

$$\lim_{M\to\infty} \int_D w_\ell^M(x,t)\mathrm{d}x = -\frac{\partial u}{\partial \overrightarrow{\mathbf{n}}}(z_\ell).$$

Proof. The regularity follows from those of u_ℓ^M and ψ_ℓ^M. Since ψ_ℓ^M are linear combinations of harmonic functions, they satisfy the equations ${}^C D_t^\alpha \psi_\ell^M - \triangle \psi_\ell^M = 0$. Hence, w_ℓ^M are weak solutions of ${}^C D_t^\alpha w_\ell^M - \triangle w_\ell^M = 0$, $(x,t) \in \Omega \times (0,T)$ subject to the boundary condition $w_\ell^M|_{\partial\Omega} = \psi_\ell^M$ and the initial condition $w_\ell^M(\cdot,0) = 0$. Then for each $v \in L^2(0,T; H_0^1(\Omega))$,

$$\int_0^t \int_\Omega ({}^C D_\tau^\alpha w_\ell^M)v + \nabla w_\ell^M \cdot \nabla v \, \mathrm{d}x \, \mathrm{d}\tau = 0. \tag{3.2}$$

A direct calculation gives

$$
\begin{aligned}
\int_0^t \int_D w_\ell^M(x,\tau) \, \mathrm{d}x \, \mathrm{d}\tau &= \int_0^t \int_D w_\ell^M(x,t-\tau) \, \mathrm{d}x \, \mathrm{d}\tau \\
&= \int_0^t \int_\Omega [{}^C D_t^\alpha u(x,\tau) - \triangle u(x,\tau)] w_\ell^M(x,t-\tau) \, \mathrm{d}x \, \mathrm{d}\tau \\
&:= I_1 + I_2.
\end{aligned}
$$

For I_1, by the regularity of the functions w_ℓ^M and u, it holds that

$$
\begin{aligned}
I_1 &= \int_0^t \int_\Omega {}^C D_t^\alpha u(x,\tau) w_\ell^M(x,t-\tau) \, \mathrm{d}x \, \mathrm{d}\tau = \int_\Omega {}^C D_t^\alpha u(x,t) * w_\ell^M(x,t) \, \mathrm{d}x \\
&= \int_\Omega \frac{t^{-\alpha}}{\Gamma(1-\alpha)} * \frac{\partial u}{\partial t}(x,t) * w_\ell^M(x,t) \, \mathrm{d}x = \int_\Omega \frac{t^{-\alpha}}{\Gamma(1-\alpha)} * \left(\frac{\partial u}{\partial t}(x,t) * w_\ell^M(x,t) \right) \, \mathrm{d}x,
\end{aligned}
$$

where $*$ represents the convolution in t. Due to the zero initial conditions of u and w_ℓ^M, we have

$$\frac{\partial u}{\partial t}(x,t) * w_\ell^M(x,t) = u(x,t) * \frac{\partial w_\ell^M}{\partial t}(x,t).$$

Hence,

$$
\begin{aligned}
I_1 &= \int_\Omega \frac{t^{-\alpha}}{\Gamma(1-\alpha)} * \frac{\partial w_\ell^M}{\partial t}(x,t) * u(x,t) \, \mathrm{d}x = \int_\Omega {}^C D_t^\alpha w_\ell^M * u(x,t) \, \mathrm{d}x \\
&= \int_0^t \int_\Omega {}^C D_t^\alpha w_\ell^M(x,t-\tau) u(x,\tau) \, \mathrm{d}x \, \mathrm{d}\tau.
\end{aligned}
$$

For the term I_2, Green's first formula and the boundary condition of w_ℓ^M give that

$$
\begin{aligned}
I_2 &= \int_0^t \int_\Omega -\triangle u(x,\tau) w_\ell^M(x,t-\tau) \, \mathrm{d}x \, \mathrm{d}\tau \\
&= \int_0^t \int_\Omega \nabla u(x,\tau) \cdot \nabla w_\ell^M(x,t-\tau) \, \mathrm{d}x \, \mathrm{d}\tau - \int_0^t \int_{\partial\Omega} \frac{\partial u}{\partial \overrightarrow{\mathbf{n}}}(x,\tau) \psi_\ell^M(x) \, \mathrm{d}x \, \mathrm{d}\tau.
\end{aligned}
$$

5

The results of I_1 and I_2, (3.2) and the definition of ψ_ℓ^M now show that

$$
\int_0^t \int_D w_\ell^M(x,\tau) \,\mathrm{d}x\,\mathrm{d}\tau = \int_0^t \int_\Omega \left[{}^C D_t^\alpha w_\ell^M(x,t-\tau)u(x,\tau) + \right.
$$
$$
\left. \nabla w_\ell^M(x,t-\tau)\cdot\nabla u(x,\tau) \right]\,\mathrm{d}x\,\mathrm{d}\tau
$$
$$
- \int_0^t \int_{\partial\Omega} \frac{\partial u}{\partial\overrightarrow{\mathbf{n}}}(x,\tau)\psi_\ell^M(x)\,\mathrm{d}x\,\mathrm{d}\tau
$$
$$
= - \int_0^t \sum_{m=1}^M c_m^c(\tau)\xi_m^c(z_\ell) + c_m^s(\tau)\xi_m^s(z_\ell)\,\mathrm{d}\tau,
$$

where $c_m^{\{c,s\}}(\tau)$ are the Fourier coefficients of $\frac{\partial u}{\partial\overrightarrow{\mathbf{n}}}(x,\tau)$ with respect to the basis $\{\xi_m^{\{c,s\}}(x) : m \in \mathbb{N}\}$ in $L^2(\partial\Omega)$. Taking derivative with respect to t in the above yields

$$
\int_D w_\ell^M(x,t) \,\mathrm{d}x = - \sum_{m=1}^M [c_m^c(t)\xi_m^c(z_\ell) + c_m^s(t)\xi_m^s(z_\ell)],
$$

which together with the pointwise convergence of the Fourier series gives

$$
\lim_{M\to\infty} \int_D w_\ell^M(x,t) \,\mathrm{d}x = - \frac{\partial u}{\partial\overrightarrow{\mathbf{n}}}(z_\ell,t)
$$

and completes the proof. $\qquad\square$

Since $\psi_\ell^M \in L^2(\Omega)$, we can represent its Fourier expansion as $\psi_\ell^M = \sum_{n=1}^\infty a_{\ell,n}^M \varphi_n$. This result, Lemma 2.1, (2.3) and [6, Theorem 3.1] lead to the following corollary.

Corollary 3.1. *The spectral representation of w_ℓ^M defined by (3.1) is*

$$
w_\ell^M(x,t) = \sum_{n=1}^\infty a_{\ell,n}^M [1 - E_{\alpha,1}(-\lambda_n t^\alpha)]\varphi_n(x), \tag{3.3}
$$

where

$$
a_{\ell,n} := \lim_{M\to\infty} a_{\ell,n}^M = (w_n/\sqrt{\lambda_n})\, J_{m+1}(\sqrt{\lambda_n})\, \xi_m^{\{c,s\}}(z_\ell). \tag{3.4}
$$

3.2 Uniqueness theorem

Theorem 3.1. *Denote the solutions of (1.1) with respect to D_1 and D_2 by u_j, $j = 1,2$, and $z_1 = (\cos\theta_1, \sin\theta_1)$, $z_2 = (\cos\theta_2, \sin\theta_2)$ satisfy the condition*

$$
\theta_1 - \theta_2 \notin \pi\mathbb{Q} \tag{3.5}
$$

where $\mathbb{Q}$ is the set of rational numbers. Then

$$
\frac{\partial u_1}{\partial\overrightarrow{\mathbf{n}}}(z_\ell,t) = \frac{\partial u_2}{\partial\overrightarrow{\mathbf{n}}}(z_\ell,t),\ \ t \in [0,T],\ \ell = 1,2
$$

implies that $D_1 = D_2$.

6

Proof. Without loss of generality we can let $\theta_1 = 0$. By Lemma 3.1 and (3.3), we obtain

$$\sum_{n=1}^{\infty} a_{\ell,n}[1 - E_{\alpha,1}(-\lambda_n t^\alpha)] \left(\int_{D_1} \varphi_n(x) \, \mathrm{d}x - \int_{D_2} \varphi_n(x) \, \mathrm{d}x \right) = 0, \quad t \in [0,T], \ \ell = 1, 2. \tag{3.6}$$

The analyticity of the Mittag-Leffler function $E_{\alpha,1}(-\lambda_n t^\alpha)$ gives

$$\sum_{n=1}^{\infty} a_{\ell,n} I_n [1 - E_{\alpha,1}(-\lambda_n t^\alpha)] = 0, \quad t \in [0, \infty), \tag{3.7}$$

where

$$I_n := \int_{D_1} \varphi_n(x) \, \mathrm{d}x - \int_{D_2} \varphi_n(x) \, \mathrm{d}x.$$

Denoting the distinct eigenvalues of the Laplacian again by $\{\lambda_k : k \in \mathbb{N}^+\}$ and taking the Laplace transform $t \to s$ in (3.7), we have

$$\sum_{k=1}^{\infty} \left(\sum_{\lambda_n = \lambda_k} a_{\ell,n} I_n \right) \frac{\lambda_k}{(s^\alpha + \lambda_k)} = 0, \quad \mathrm{Re}\{s\} > 0.$$

Letting $\eta = s^\alpha$ shows that the function

$$\Xi(\eta) := \sum_{k=1}^{\infty} \left(\sum_{\lambda_n = \lambda_k} a_{\ell,n} I_n \right) \frac{\lambda_k}{\eta + \lambda_k} = 0, \quad \mathrm{Re}\{\eta\} > 0, \tag{3.8}$$

is analytic in η with poles at $\eta = \{-\lambda_k\}$ and corresponding residues $\{\lambda_k \sum_{\lambda_n = \lambda_k} a_{\ell,n} I_n\}_k$. However, since $\Xi(\eta)$ vanishes identically for η real and positive, it follows that these residues must be zero. Then by the strict positivity of λ_k we see that $\sum_{\lambda_n = \lambda_k} a_{\ell,n} I_n = 0$ for $\ell = 1, 2$ and each eigenvalue λ_k of the Laplacian.

For a fixed eigenvalue λ_k, denote its corresponding eigenfunctions by φ_{n_k} and φ_{n_k+1}. These have different phases and hence

$$\sum_{n = n_k, n_k+1} a_{\ell,n} I_n = 0, \quad \ell = 1, 2. \tag{3.9}$$

For the case of $\phi_{n_k} = 0$, since $\theta_1 = 0$, $\theta_1 - \theta_2 \notin \pi\mathbb{Q}$, then (3.4) implies $a_{1,n_k} \neq 0$, $a_{1,n_k+1} = 0$ and $a_{2,n_k+1} \neq 0$. Inserting this into (3.9) yields $I_{n_k} = 0$. The above result means $a_{2,n_k+1} I_{n_k+1} = 0$, which together with $a_{2,n_k+1} \neq 0$ gives $I_{n_k+1} = 0$. Analogously, for the case of $\phi_{n_k} = \pi/2$, we can prove $I_{n_k} = I_{n_k+1} = 0$. Hence, we can conclude that for each eigenvalue $\lambda_k \in \{\lambda_n : n \in \mathbb{N}^+\}$, $I_{n_k} = I_{n_k+1} = 0$, which means

$$\int_{D_1} \varphi_n(x) \, \mathrm{d}x - \int_{D_2} \varphi_n(x) \, \mathrm{d}x = \int_\Omega (\chi_{D_1} - \chi_{D_2}) \varphi_n(x) \, \mathrm{d}x = 0, \ n \in \mathbb{N}^+.$$

This result, the completeness of $\{\varphi_n(x) : n \in \mathbb{N}^+\}$ and the continuity of the boundaries of D_1 and D_2 give that $D_1 = D_2$. $\qquad\square$

In practice, it is certainly possible that the measured data can only be obtained after some initial time T_0 has elapsed, i.e. only $g_\ell(t)$, $t \in [T_0, T]$ is obtained. Hence, the following corollary is important; its proof follows immediately from the analyticity of the Mittag-Leffler function and the proof of Theorem 3.1.

7

Corollary 3.2. *With the same conditions of Theorem 3.1 and a constant $T_0 \in (0, T)$,*

$$\frac{\partial u_1}{\partial \overrightarrow{\mathbf{n}}}(z_\ell, t) = \frac{\partial u_2}{\partial \overrightarrow{\mathbf{n}}}(z_\ell, t) \ on \ [T_0, T], \ \ell = 1, 2$$

will also imply $D_1 = D_2$.

Remark 3.1. *The condition $\theta_1 - \theta_2 \notin \pi\mathbb{Q}$ is almost impossible to be satisfied in practice. However, as we will show, in the numerical section, we only use the partial sum of the solution series to approximate the exact spectral representation. By taking a truncated basis, that is spectral cut-off of the functions used to represent ∂D, we can show that satisfying (3.5) is feasible. Since in this case the number of eigenvalues is finite, the upper bound M of the degrees for the corresponding Bessel function will also be finite. Hence, in numerical reconstructions the condition $\theta_1 - \theta_2 \notin \pi\mathbb{Q}$ can be weakened to*

$$\sin m(\theta_1 - \theta_2) \neq 0, \quad m = 1, 2, \ldots, M. \tag{3.10}$$

3.3 The operators G and G'

In order to use Newton's method to recover D, we need to construct the operator G which maps D to the flux data $\frac{\partial u}{\partial \overrightarrow{\mathbf{n}}}(z_\ell, t)$ then compute and demonstrate needed properties of its derivative G'. In particular, to show the injectivity of G'.

Recall that we have assumed the boundary of D is star-like, i.e.

$$\partial D = \{q(\theta)(\cos\theta, \sin\theta)^\top : \theta \in [0, 2\pi]\}.$$

Then by (2.3), the representation of $u(x, t)$ will be

$$
\begin{aligned}
u(x, t) &= \sum_{n=1}^{\infty} \left(\int_0^t \int_\Omega \chi_D \varphi_n(y)(t - \tau)^{\alpha-1} E_{\alpha,\alpha}(-\lambda_n(t-\tau)^\alpha) \, \mathrm{d}y \, \mathrm{d}\tau \right) \varphi_n(x) \\
&= \sum_{n=1}^{\infty} \lambda_n^{-1}(1 - E_{\alpha,1}(-\lambda_n t^\alpha)) \varphi_n(r, \theta) \int_0^{2\pi} \int_0^{q(s)} \varphi_n(\rho, s) \rho \, \mathrm{d}\rho \, \mathrm{d}s.
\end{aligned}
\tag{3.11}
$$

Now we can define the operator G as $G : q \mapsto (\partial_r u(1, \theta_1, t), \partial_r u(1, \theta_2, t))$, where θ_ℓ, $\ell = 1, 2$ are the polar angles of the observation points z_ℓ on $\partial\Omega$. The polar representation of φ_n is $\varphi_n(r, \theta) = w_n J_m(\sqrt{\lambda_n}\, r)\cos(m\theta + \phi_n)$ and we use the relation $J'_m(z) = -J_{m+1}(z) + \frac{m}{z}J_m(z)$ and the fact that $\sqrt{\lambda_n}$ is a zero of the m-th Bessel function J_m to see that the radial derivative of the radial part of φ_n is $w_n \sqrt{\lambda_n} J_{m+1}(\sqrt{\lambda_n})$. Thus a direct calculation from (3.11) yields the ℓ-th component of G as

$$G_\ell(q)(t) = \sum_{n=1}^{\infty} b_n [1 - E_{\alpha,1}(-\lambda_n t^\alpha)] \cos(m\theta_\ell - \phi_n) \int_0^{2\pi} \Phi_n(q(s)) \cos(ms - \phi_n) \, \mathrm{d}s, \tag{3.12}$$

where

$$b_n = -w_n^2 \lambda_n^{-3/2} J_{m+1}(\sqrt{\lambda_n}), \quad \Phi_n(x) := \int_0^{x\sqrt{\lambda_n}} \rho \, J_m(\rho) \, \mathrm{d}\rho.$$

To compute w_n we require the integral $\int_0^{2\pi}\int_0^1 \rho J_m(\sqrt{\lambda_n}\rho)^2 d\rho$. The recursion formulae $[t^{-m}J_m(t)]' = -t^{-m}J_{m+1}(t)$ and $[t^m J_m(t)]' = t^m J_{m-1}(t)$ give the relations $2tJ_m(t)^2 = [t^2 J_m(t)^2 - J_{m+1}J_{m-1}]'$ and $J_{m-1}(t) = J'_m(t) = -J_{m+1}(t)$. These and the fact that $J_m(\sqrt{\lambda_n}) = 0$ show that $\int_0^{2\pi}\int_0^1 \rho J_m(\sqrt{\lambda_n}\rho)^2 d\rho =$

$\frac{1}{2}J_{m+1}(\sqrt{\lambda_n}\rho)^2$. Thus $\|\phi_n\|_2^2 = 1/w_n^2 = \frac{1}{2}\eta_n\pi J_{m+1}(\sqrt{\lambda_n}\rho)^2$ where $\eta_n = 1$ if $m(n) = 0$ and $\frac{1}{2}$ if $m > 0$. Combining all of these shows that

$$b_n = \frac{1}{\eta_n\pi\lambda_n^{3/2}J_{m+1}(\sqrt{\lambda_n})}.$$

These computations mirror those of [6] for the parabolic case. From (3.12), with the notation $\sum'$ which indicates the index over distinct eigenvalues, we obtain

$$\begin{aligned}
G_\ell(q)(t) = \sum_{n=1}^{\infty}{}' b_n(1 - E_{\alpha,1}(-\lambda_n t^\alpha)) \Big[& \cos(m\theta_\ell) \int_0^{2\pi} \Phi_n(q(s))\cos(ms)\,\mathrm{d}s \\
& + \sin(m\theta_\ell) \int_0^{2\pi} \Phi_n(q(s))\sin(ms)\,\mathrm{d}s \Big] \\
= \sum_{n=1}^{\infty}{}' b_n(1 - E_{\alpha,1}(-\lambda_n t^\alpha)) & \int_0^{2\pi} \Phi_n(q(s))\cos(m(s - \theta_\ell))\,\mathrm{d}s,
\end{aligned} \tag{3.13}$$

and

$$G_\ell'[q].h(t) = \sum_{n=1}^{\infty}{}' \lambda_n b_n(1 - E_{\alpha,1}(-\lambda_n t^\alpha)) \int_0^{2\pi} q(s)J_m(\sqrt{\lambda_n}q(s))\cos(m(s - \theta_\ell))h(s)\,\mathrm{d}s, \tag{3.14}$$

where h denotes the direction operated by $G_\ell'[q]$. We can now define G and G' by

Definition 3.1.
$$G(q)(t) = \begin{bmatrix} G_1(q)(t) \\ G_2(q)(t) \end{bmatrix}, \quad G'[q].h(t) = \begin{bmatrix} G_1'[q].h(t) \\ G_2'[q].h(t) \end{bmatrix},$$

where G_ℓ, G_ℓ', $\ell = 1, 2$ are defined in (3.13) and (3.14).

3.4   Injectivity of G'

We are now able to show the injectivity of G'.

Corollary 3.3. *Under the condition* (3.5), $G'[q].h(t) = 0$ *implies that* $h = 0$.

Proof. $G'[q].h(t) = 0$ leads to $G_1'[q].h(t) = G_2'[q].h(t) = 0$. Following the proof of Theorem 3.1, we have
$$\int_0^{2\pi} q(s)J_m(\sqrt{\lambda_n}q(s))\cos(m(s - \theta_\ell))h(s)\,\mathrm{d}s = 0, \quad n \in \mathbb{N}^+, \ \ell = 1, 2.$$

Applying the proof in [6, Section 4] shows that $h = 0$. $\qquad\square$

An interesting question arises if the source contains a time-dependent term; for example, $a(t)\chi_D$ where the time dependent function $a(t)$ has to be determined in addition to D. Even in the case $a(t)$ is constant more than two observation points would now be needed, but it is easy to see that three would suffice. It is a reasonable conjecture that three points would also suffice to determine in addition $a(t)$ although this isn't immediately clear. Although the unknown source would still give rise to a linear fractional equation with the advantage that representation results would still hold, the fact that the two unknowns $a(t)$ and D are coupled in a nonlinear fashion adds considerable complexity to the new operators G and G'.

4 Numerical reconstruction

4.1 Iterative algorithm

Using the operator G, the reconstruction approach requires the solution of the equation

$$g - G(q) = 0,$$

where g is the measured data. Newton's method gives the iteration scheme

$$q_{n+1} = q_n + [(G'(q_n))^* \, G'(q_n)]^{-1} (G'(q_n))^*(g - G(q_n)).$$

Here, Corollary 3.3 ensures that $(G'(q_n))^* \, G'(q_n)$ is invertible. However, the ill-posedness will guarantee that the singular values of the matrix $[(G'(q_n))^* \, G'(q_n)]$ will tend to zero rapidly, any noise in the measured data g_δ will cause large errors in the approximation. Hence, some regularization scheme must be included and we use Tikhonov's approach adding a penalty matrix P with a regularized parameter β. Now the iteration becomes one of the Levenberg-Marquardt-type:

$$q_{n+1} = q_n + [(G'(q_n))^* \, G'(q_n) + \beta P]^{-1} (G'(q_n))^*(g^\delta - G(q_n)). \tag{4.1}$$

Here, g^δ denotes the perturbed measured data with $\|(g - g^\delta)/g\|_{C(0,T)} \le \delta$, q_n is the n-th approximation of the radial term of the star-like boundary, β is the regularized parameter and P is the penalized matrix. In this section, we only consider the unknown q to be taken from the trigonometric polynomial space with dimension up to degree M, i.e.

$$q(\theta) = \frac{1}{2}q_0 + \sum_{n=1}^{M} \left(q_n^c \cos n\theta + q_n^s \sin n\theta \right).$$

As will be seen, the effective value for M that can be obtained will be quite small. This itself provides a regularization by spectral cut off, but if used alone it leads to a quite limited regularization possibility; hence the combination with (4.1).

We also want to ensure the approximated q_n is sufficiently smooth and so we set the penalty term be the H^2 semi-norm of q_n, which implies that P is a $(2M+1) \times (2M+1)$ diagonal matrix with

$$P_{1,1} = 1, \; P_{i+1,i+1} = P_{i+M+1,i+M+1} = i^2, \; i = 1, \ldots, M.$$

The stopping criterion used was $\|g^\delta - G(q_n)\|_{L^2(0,T)} \le \epsilon$, $\epsilon = O(\delta)$. A good initial approximation is often essential for the convergence of Newton schemes in such interior domain reconstructions and the current case is no different. Fortunately, we have a simple method of achieving this as noted in [6]. We take q_0 to be a circle of radius $\bar{r}$ with centre $\bar{x} = (\bar{x}_1, \bar{x}_2)$. An extended circular source has exactly the same boundary effect as a delta-function point source at its centre. Such a pole would generate a disturbance equal to $G_\alpha(\bar{x} - z, t)$ where G_α is the fundamental solution for the subdiffusion operator in (1.1). This solution is available as a Wright function, $G_\alpha(x, t) = t^{-\alpha/2}M(|x|/t^{\alpha/2})$ where $M(z) = \sum_0^\infty \frac{(-z)^n}{n!\Gamma(1 - \frac{\alpha}{2}(n+1))}$, see [12]. However, we do not require such precision for the initial approximation purpose. We can take the time-independent version by approximation of the steady state values for each flux $g_\ell(t_\infty)$. This gives m values at positions z_ℓ and we simply perform a least-squares fit to obtain the centre $\bar{x}$ and weight $\bar{\rho}$ of the pole based on Laplace equation for a circle. Then, since $\bar{\rho} = \pi \bar{r}^2$, we readily obtain our approximating circle. In the case of only two observation points there is insufficient information in general and then we simply assume the approximating circle has centre the origin.

4.2   Decomposition of G and G'

From the definitions of G and G' we can see the convergence rates of their series representations should be slow since the time-dependent term $1 - E_{\alpha,1}(-\lambda_n t^\alpha)$ does not converge to zero for n large. Hence, we split G, G' into their steady states and transient components as

$$G_\ell(q)(t) = \frac{\partial v}{\partial \overrightarrow{\mathbf{n}}}(z_\ell) - \sum_{n=1}^{\infty}{}' b_n E_{\alpha,1}(-\lambda_n t^\alpha) \int_0^{2\pi} \Phi_n(q(s)) \cos\left(m(s - \theta_\ell)\right) \, \mathrm{d}s,$$

$$G'_\ell(q)(t) = \frac{\partial}{\partial q}\left(\frac{\partial v}{\partial \overrightarrow{\mathbf{n}}}(z_\ell)\right)$$
$$- \sum_{n=1}^{\infty}{}' \lambda_n b_n E_{\alpha,1}(-\lambda_n t^\alpha) \int_0^{2\pi} q(s) J_m(\sqrt{\lambda_n}q(s)) \cos\left(m(s - \theta_\ell)\right) h(s) \, \mathrm{d}s,$$

where v is the solution of the equation

$$\begin{cases} -\triangle v(x) = \chi_D, & x \in \Omega; \\ \quad\;\; v(x) = 0, & x \in \partial\Omega. \end{cases}$$

From [7] we can obtain $\frac{\partial v}{\partial \overrightarrow{\mathbf{n}}}(z_\ell)$ and $\frac{\partial}{\partial q}\left(\frac{\partial v}{\partial \overrightarrow{\mathbf{n}}}(z_\ell)\right)$ from the following Fourier expansions

$$\frac{\partial v}{\partial \overrightarrow{\mathbf{n}}}(z_\ell) = \frac{a_0}{2} + \sum_{n=1}^{\infty}\left(a_n^c \cos n\theta_\ell + a_n^s \sin n\theta_\ell\right),$$

$$\frac{\partial}{\partial q}\left(\frac{\partial v}{\partial \overrightarrow{\mathbf{n}}}(z_\ell)\right) = \frac{b_0}{2} + \sum_{n=1}^{\infty}\left(b_n^c \cos n\theta_\ell + b_n^s \sin n\theta_\ell\right),$$

where

$$a_n^c = \frac{1}{(n+2)\pi} \int_0^{2\pi} [q(\theta)]^{n+2} \cos n\theta \, \mathrm{d}\theta, \qquad a_n^s = \frac{1}{(n+2)\pi} \int_0^{2\pi} [q(\theta)]^{n+2} \sin n\theta \, \mathrm{d}\theta,$$

$$b_n^c = \frac{1}{\pi} \int_0^{2\pi} [q(\theta)]^{n+1} \cos n\theta \, \mathrm{d}\theta, \qquad b_n^s = \frac{1}{\pi} \int_0^{2\pi} [q(\theta)]^{n+1} \sin n\theta \, \mathrm{d}\theta.$$

4.3   Forward problem and L^1 time-stepping

To obtain the measured data g and also to compute the forward map we need to solve the (1.1) numerically. The spectral representation of the solution $u(x, t)$ gives insight to the problem but as our forcing function is discontinuous, the convergence, in particular that of the boundary derivative, is very slow. This forces an extremely large number of eigenfunctions to be taken in order to obtain sufficient accuracy. As an alternative to the spectral representation we use a finite difference representation in space and the L^1 time-stepping method [8] to discretize the fractional derivative

$^CD_t^\alpha$

$$^CD_t^\alpha u(x, t_N) = \frac{1}{\Gamma(1-\alpha)} \sum_{j=0}^{N-1} \int_{t_j}^{t_{j+1}} \frac{\partial u(x,s)}{\partial s}(t_N - s)^{-\alpha}\, ds$$

$$\approx \frac{1}{\Gamma(1-\alpha)} \sum_{j=0}^{N-1} \frac{u(x, t_{j+1}) - u(x, t_j)}{\tau} \int_{t_j}^{t_{j+1}} (t_N - s)^{-\alpha} ds$$

$$= \sum_{j=0}^{N-1} b_j \frac{u(x, t_{N-j}) - u(x, t_{N-j-1})}{\tau^\alpha}$$

$$= \tau^{-\alpha}[b_0 u(x, t_N) - b_{N-1} u(x, t_0) + \sum_{j=1}^{N-1}(b_j - b_{j-1})u(x, t_{N-j})],$$

where τ is the step size of the uniform partition on t and

$$b_j = ((j+1)^{1-\alpha} - j^{1-\alpha})/\Gamma(2-\alpha), \ j = 0, 1, \ldots, N-1.$$

For the Laplace operator $\triangle$, the polar form $\triangle u = \frac{\partial^2 u}{\partial r^2} + \frac{1}{r}\frac{\partial u}{\partial r} + \frac{1}{r^2}\frac{\partial^2 u}{\partial \theta^2}$ is used since the domain Ω is the unit disc in $\mathbb{R}^2$. With uniformly partitions $\{r_l\}$, $\{\theta_k\}$ on the radius $r \in (0,1)$ and the angle $\theta \in [0, 2\pi)$ respectively, the discretized form of $-\triangle$ is

$$-\triangle u(l, k, t_N) = -\frac{1}{h_r^2}[u(l+1, k, t_N) + u(l-1, k, t_N) - 2u(l, k, t_N)]$$

$$- \frac{1}{2lh_r^2}[u(l+1, k, t_N) - u(l-1, k, t_N)]$$

$$- \frac{1}{l^2 h_r^2 h_\theta^2}[u(l, k+1, t_N) + u(l, k-1, t_N) - 2u(l, k, t_N)]$$

$$= (-\frac{1}{h_r^2} + \frac{1}{2lh_r^2})u(l-1, k, t_N) + (-\frac{1}{h_r^2} - \frac{1}{2lh_r^2})u(l+1, k, t_N)$$

$$+ (\frac{2}{h_r^2} + \frac{2}{l^2 h_r^2 h_\theta^2})u(l, k, t_N) - \frac{u(l, k+1, t_N)}{l^2 h_r^2 h_\theta^2} - \frac{u(l, k-1, t_N)}{l^2 h_r^2 h_\theta^2},$$

where $u(l, k, t_N) = u(r_l, \theta_k, t_N)$, and h_r, h_θ are the step sizes of the partitions on r and θ respectively. Hence, the finite difference scheme of the forward problem of (1.1) is

$$(\tau^{-\alpha}b_0 + \frac{2}{h_r^2} + \frac{2}{l^2 h_r^2 h_\theta^2})u(l, k, t_N) + (-\frac{1}{h_r^2} + \frac{1}{2lh_r^2})u(l-1, k, t_N)$$

$$+ (-\frac{1}{h_r^2} - \frac{1}{2lh_r^2})u(l+1, k, t_N) + (-\frac{1}{l^2 h_r^2 h_\theta^2})u(l, k+1, t_N) + (-\frac{1}{l^2 h_r^2 h_\theta^2})u(l, k-1, t_N) \quad (4.2)$$

$$= \tau^{-\alpha}b_{N-1}u(l, k, t_0) - \sum_{j=1}^{N-1} \tau^{-\alpha}(b_j - b_{j-1})u(l, k, t_{N-j}) + \chi_D(l, k).$$

Remark 4.1. *For the truncation errors of the discretization schemes for $^CD_t^\alpha u(x, t_N)$ and $-\triangle u(l, k, t_N)$,*

12

we have

$$
{}^{C}D_{t}^{\alpha}u(x,t_{N})-\tau^{-\alpha}[b_{0}u(x,t_{N})-b_{N-1}u(x,t_{0})+\sum_{j=1}^{N-1}(b_{j}-b_{j-1})u(x,t_{N-j})]
$$

$$
=\frac{1}{\Gamma(1-\alpha)}\sum_{j=0}^{N-1}\int_{t_{j}}^{t_{j+1}}\left[\frac{\partial u(x,s)}{\partial s}-\frac{u(x,t_{j+1})-u(x,t_{j})}{\tau}\right](t_{N}-s)^{-\alpha}\,ds
$$

$$
=\frac{1}{\Gamma(1-\alpha)}\sum_{j=0}^{N-1}\int_{t_{j}}^{t_{j+1}}O(\tau)(t_{N}-s)^{-\alpha}\,ds=\frac{O(\tau)}{\Gamma(1-\alpha)}\int_{0}^{t_{N}}(t_{N}-s)^{-\alpha}\,ds
$$

$$
=O(\tau),
$$

and

$$
-\triangle u(l,k,t_{N})+\frac{1}{h_{r}^{2}}[u(l+1,k,t_{N})+u(l-1,k,t_{N})-2u(l,k,t_{N})]
$$

$$
+\frac{1}{2lh_{r}^{2}}[u(l+1,k,t_{N})-u(l-1,k,t_{N})]+\frac{1}{l^{2}h_{r}^{2}h_{\theta}^{2}}[u(l,k+1,t_{N})+u(l,k-1,t_{N})-2u(l,k,t_{N})]
$$

$$
=\frac{1}{h_{r}^{2}}[u(l+1,k,t_{N})+u(l-1,k,t_{N})-2u(l,k,t_{N})]-\frac{\partial^{2}u}{\partial r^{2}}(l,k,t_{N})
$$

$$
+\frac{1}{2lh_{r}^{2}}[u(l+1,k,t_{N})-u(l-1,k,t_{N})]-\frac{1}{r}\frac{\partial u}{\partial r}(l,k,t_{N})
$$

$$
+\frac{1}{l^{2}h_{r}^{2}h_{\theta}^{2}}[u(l,k+1,t_{N})+u(l,k-1,t_{N})-2u(l,k,t_{N})]-\frac{1}{r^{2}}\frac{\partial^{2}u}{\partial\theta^{2}}(l,k,t_{N})
$$

$$
=O(h_{r})+O(h_{r}^{2})+O(h_{\theta})=O(h_{r}+h_{\theta}).
$$

Hence, the truncation errors vanish as $\tau, h_{r}, h_{\theta} \to 0$, which indicates the consistency of the finite difference scheme (4.2).
Returning to (4.2), the left side can be written as $A\vec{u}_{N}$, where the vector $\vec{u}_{N}$ denotes the solution vector at $t = t_{N}$. Since

$$
\left(\tau^{-\alpha}b_{0}+\frac{2}{h_{r}^{2}}+\frac{2}{l^{2}h_{r}^{2}h_{\theta}^{2}}\right)-\left|-\frac{1}{h_{r}^{2}}+\frac{1}{2lh_{r}^{2}}\right|-\left|\frac{1}{h_{r}^{2}}+\frac{1}{2lh_{r}^{2}}\right|-\left|\frac{1}{l^{2}h_{r}^{2}h_{\theta}^{2}}\right|-\left|\frac{1}{l^{2}h_{r}^{2}h_{\theta}^{2}}\right|=\tau^{-\alpha}b_{0}>0,
$$

the matrix A is strictly diagonally dominant. By Gershgorin circle theorem, we have that for any eigenvalue λ of A, it satisfies

$$
\left|\lambda-\tau^{-\alpha}b_{0}-\frac{2}{h_{r}^{2}}-\frac{2}{l^{2}h_{r}^{2}h_{\theta}^{2}}\right|\leq\left|-\frac{1}{h_{r}^{2}}+\frac{1}{2lh_{r}^{2}}\right|+\left|\frac{1}{h_{r}^{2}}+\frac{1}{2lh_{r}^{2}}\right|+\left|\frac{1}{l^{2}h_{r}^{2}h_{\theta}^{2}}\right|+\left|\frac{1}{l^{2}h_{r}^{2}h_{\theta}^{2}}\right|
$$

$$
=\frac{2}{h_{r}^{2}}+\frac{2}{l^{2}h_{r}^{2}h_{\theta}^{2}},
$$

which implies $\lambda \geq \tau^{-\alpha}b_{0}$. The small time step size τ ensures that $\lambda > 1$. Hence, we have proved that for each eigenvalue λ of A, $\lambda > 1$ is valid. This gives the stability of the finite difference scheme (4.2).

4.4 Numerical results

The purpose of this section is to investigate our ability to perform reconstructions and in particular to investigate the difference as a function of α. We will also look at the effect of different placements of the measurements points, of the noise level in the data. This will be accomplished by a series of experiments to be outlined below.

In all the figures to be shown, the legend is the following: the (blue) dotted line is the exact curve; the (red) dashed line is the reconstructed curve; and the (blue) solid circle with the two black dots representing the exterior boundary $\partial\Omega$ and the observation points z_ℓ respectively.

We set $\alpha = 0.9$ and the final time $T = 1$. For the regularized parameter β, large values will smooth the approximation excessively and small values will not sufficiently correct the ill-posedness of the inverse problem. It is possible to match the value to β to the perceived noise level in the data, for example using Morozov's principle or by the L-curve method, [5], but this is always to some extent an *ad hoc* process. We suppose the data $g_\ell(t)$ has uniform random added noise of δ times the value. After several tests, we chose $\beta = 10^{-2}$ for the case of an error level $\delta = 1\%$. The results for other (inappropriate) values of β can be seen in Figure 3. Then the following experiments were constructed.

$$E_{1a}: \quad q(\theta) = 0.6 + 0.1\cos\theta + 0.1\sin 2\theta, \quad \theta_1 = \frac{15}{32}\pi, \ \theta_2 = \frac{19}{16}\pi, \ \epsilon = \delta/2;$$

$$E_{1b}: \quad q(\theta) = 0.6 + 0.1\cos\theta + 0.1\sin 2\theta, \quad \theta_1 = \frac{3}{4}\pi, \ \theta_2 = \frac{55}{32}\pi, \ \epsilon = \delta/2.$$

Experiments E_{1a} and E_{1b} have the same exact radius function $q(\theta)$. However, the locations of observation points are different and this leads to the difference between reconstructions of these two experiments. See Figure 1 for an illustration of the fact that the reconstructed domain D depends strongly on the location of the observation points.

The left figure here is with 1% noise, but actually even a significant change in the noise level (5% against 1%) has little bearing in this respect, the former being only slightly worse. The change of the observation points in E_{1b} shown in the middle and rightmost figures makes an enormous difference here; reconstructions are considerably improved.
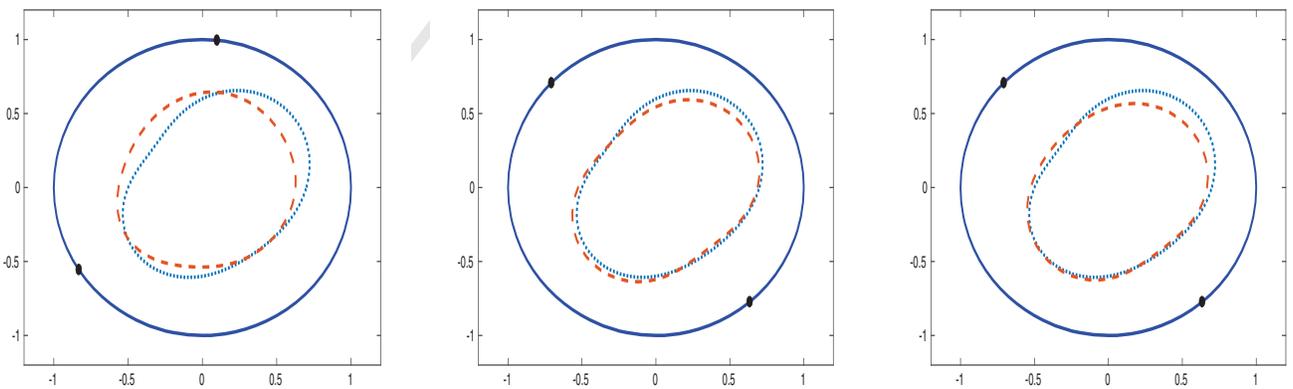

Figure 1: Exact q and numerical approximation, $\alpha = 0.9$.
Left: E_{1a}, $\delta = 1\%$; Middle: E_{1b}, $\delta = 1\%$; Right: E_{1b}, $\delta = 5\%$.

This prompts us to redo this experiments to find the relation between curve features and obser-

vation points in the reconstruction.

$$E_{2a}: \quad q(\theta) = 0.5 + 0.05\cos\theta + 0.3\sin 2\theta, \quad \theta_1 = 0, \quad \theta_2 = \frac{31}{32}\pi, \ \epsilon = \delta/10;$$

$$E_{2b}: \quad q(\theta) = 0.5 + 0.05\cos\theta + 0.3\sin 2\theta, \quad \theta_1 = \frac{23}{32}\pi, \ \theta_2 = \frac{27}{16}\pi, \ \epsilon = \delta/10.$$

The reconstruction pairs in Figure 2 express the expected outcome; both the proximity and alignment of the observation points are to the critical features of the exact q, the better is the obtained approximation.
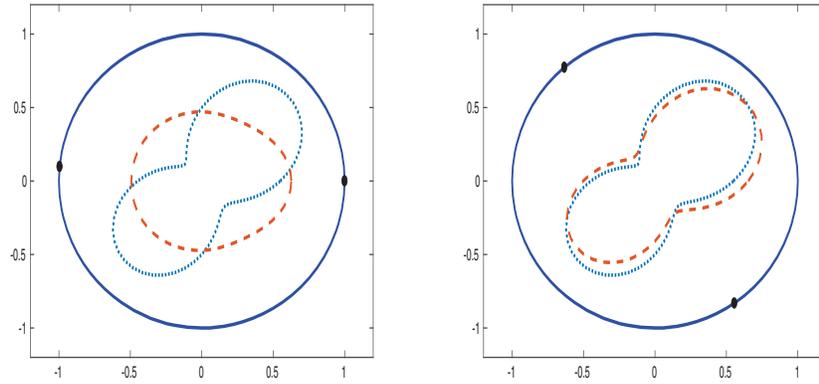

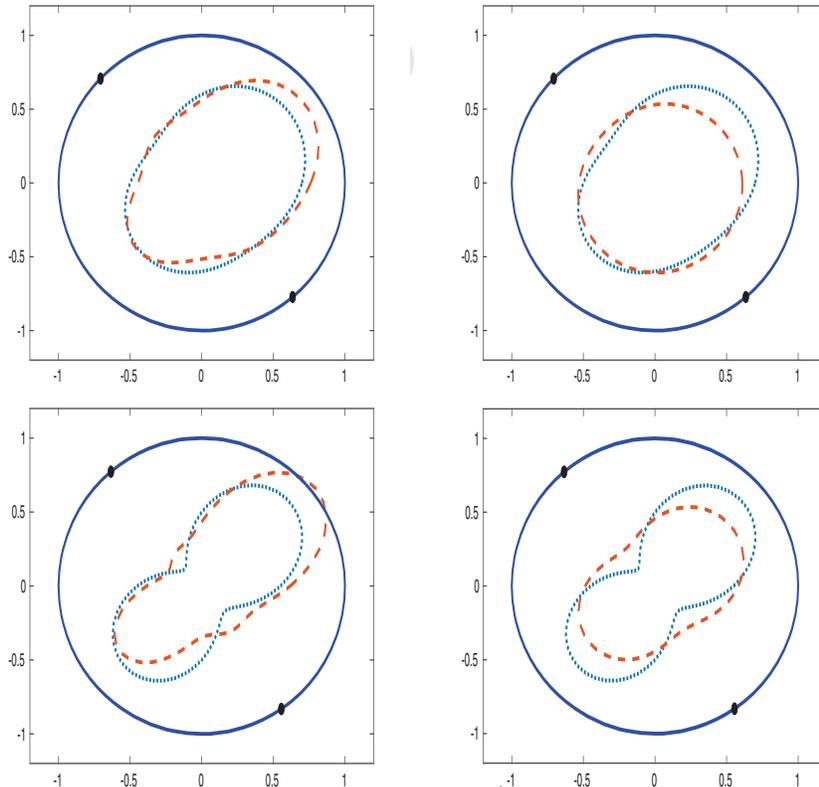Figure 2: Results of experiments E_{2a} (left) and E_{2b} (right), $\delta = 1\%$, $\alpha = 0.9$.

Figure 3: E_{1b} (top) and E_{2b} (bottom) for $\beta = 10^{-4}$ (left) and $\beta = 1$ (right) with $\delta = 1\%$.

A rigorous theoretical proof of this would be extremely useful but the observation is widely reported in other situations. For example, in inverse obstacle scattering there is a shadow region

15

	$\epsilon = \delta$	$\epsilon = \delta/5$	$\epsilon = \delta/10$
$N_G = 25$	13.589 (1 iteration)	24.904 (4 iterations)	28.714 (5 iterations)
$N_G = 50$	19.947 (1 iteration)	36.798 (3 iterations)	52.219 (5 iterations)
$N_G = 100$	34.023 (1 iteration)	88.292 (4 iterations)	107.743 (5 iterations)

Table 1: CPU times (in second) for different choices of ϵ and N_G.
Experiment E_{2b}, $\delta = 1\%$.

on the reverse side of an incident wave from a given direction. While all these problems do have strong diffusion and the theoretical ability to "wrap around" obstacles, this is still limited.

Moreover, we investigate the dependence of the running time of this algorithm on controlling parameters ϵ and N_G, where N_G means the amount of the eigenvalues we use in the approximation of the operators G and G'. The stopping criterion ϵ can affect the amount of iterations and N_G determines the cost of the calculations of the matrices $G'(q_n)$ and $G(q_n)$. Table 1 is given which displays the CPU time of the experiment E_{2b} for different choices of ϵ and N_G.

4.5 Fractional vs classical diffusion reconstructions

An obvious question is how the reconstructions will depend on the fractional diffusion parameter α. First we consider what the profile of a typical data measurement $g(t)$ should be.

The model (1.1) has the positivity property; the nonhomogeneous forcing function and initial value are nonnegative and this implies the solution $u(x,t)$ be nonnegative for all (x,t), see [11]. Thus the (exact) overposed flux values consisting of the outer normal derivative on $\partial\Omega$ will be negative for all t. In fact these values must start at 0 and monotonically increase to the steady state value predicted by the equation $-\triangle u = \chi_D$ with the same Dirichlet condition on $\partial\Omega$ as imposed by (1.1). From equation (3.3) and the monotonicity of the Mittag-Leffler function on the negative real axis the term $\sigma_{\alpha,n}(t) := 1 - E_{\alpha,1}(-\lambda_n t^\alpha)$ is monotone and the range of this is within $[0,1)$ for all t. Even if the time interval is truncated to $[0,T]$, since $\lambda_n \to \infty$ linearly in n, most of the modes will have the property that $\sigma_{\alpha,n}(t)$ covers a substantial part of the range $(0,1]$. However, this will not be independent of α as the growth of $E_{\alpha,1}(-\lambda t^\alpha)$ depends on α. The larger the α, the initially the slower, but finally the faster the decay of $E_{\alpha,1}(-\lambda t^\alpha)$ to zero. Thus, as we have seen in Figure 4, the heat equation with $\alpha = 1$ will reach steady state faster than for $\alpha < 1$ and the smaller the α the longer it will take to reach steady state. Of course the high frequency modes (large λ_n) will reach steady state much faster and this is true for all α.

The explanation of why this is important is clear from (3.3) and perhaps more apparent with the heat equation and the resulting exponential function $E_{1,1}$ although the identical argument applies to the Mittag-Leffler function $E_{\alpha,1}$ albeit to a slightly different degree. For the term $e^{-\lambda_n t}$ to remain sufficiently large to contain extractable information we require the argument $\lambda_n t$ to be sufficiently small. If $\lambda_n < \Lambda$ and $t > T_0$ then $e^{-\lambda_n t} < e^{-\Lambda T_0} < \epsilon$ for $\Lambda < -\ln(\epsilon)/T_0$ showing that for a given ϵ and value T_0 we are restricted to a maximum Λ; that is we cannot effectively use the nth eigenfunction mode in equation (3.3) if $\lambda_n > \Lambda$.

Figure 4 shows the function $g(t)$ for both $\alpha = 1$ and $\alpha = \frac{1}{2}$, for the case of a circular inclusion with centre the origin. In each case $g(t)$ goes to the same steady state value but how it approaches this is quite different. In the case of the heat equation the effective steady state is reached long before the endpoint chosen here of $T = 2$. Indeed, by $t = 0.5$, 99% of the steady state value has been achieved and is typical of the behaviour expected by the exponential term in the solution representation when $\alpha = 1$. When $\alpha = \frac{1}{2}$ the situation is quite different; the Mittag-Leffler function
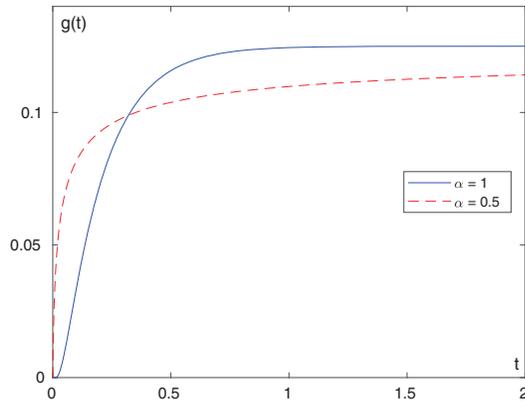
Figure 4: The data $g_\alpha(t)$.
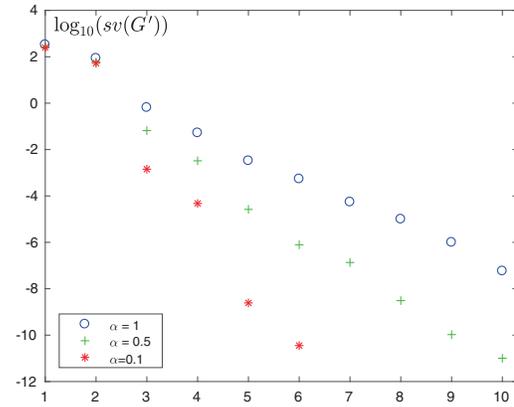
Figure 5: Singular values of G'.

decays only linearly for large (negative) values of the argument and so steady state is achieved much more slowly. In consequence, for $\alpha = 1$ only time measurements made for small t offer any utility in providing information, but for $\alpha < 1$ this is not the case (at least in theory).

What this figure illustrates is the very narrow time interval where a large part of the diffusion takes place for $\alpha < 1$ as against $\alpha = 1$ and, in fact, becomes more extreme the smaller the value of α. Thus for an source whose representation requires high frequency eigenfunctions, for a given measurement set $\{t_1, t_2, \ldots\}$, we should expect poorer reconstruction in the anomalous diffusion case over the heat equation and this effect will be greater the smaller the α. Numerical experiments bear this out.

Figure 5 displays the singular values σ_k of the operator $(G')^* \circ G'$ for experiment E_{2b}. Note the obvious exponential decay of σ_k for all α. This is to be expected due to the extreme ill-conditioning of the problem. However, the rates do depend on α; the smaller the α the greater the decay rate and hence degree of ill-conditioning. Again, this must be expected as for small α the diffusion is initially extremely rapid and the transient information cannot be adequately captured. Thus, while all cases require $g(t)$ for small values of t this is even more important the smaller the α. The slower growth of the profile $g(t)$ for larger t cannot compensate. Although this seems anomalous at first glance, the factor $1 - E_{\alpha,1}(-z)$ for large argument $z = \lambda_n t^\alpha$ approaches unity with behaviour $\frac{c_1}{z} + \frac{c_2}{z^2} + \ldots$ where $c_k = c_k(\alpha)$. Hence for modest values of t, say near $t = 1$ but large λ_n this is dominated by the first term with a rapidly diminishing contribution to further terms $1/z^2$, $1/z^3$ ... and so also offers relatively little information to be picked up from $g(t)$.

Note that while it is important to take a small step size initially in the measurement of $g(t)$ this need not be continued for the entire interval. Thus if we take say the first few measurements with $dt = 0.001$ then this can be steadily increased so that (say) over the last half of $[0, T]$ we use a step size of $dt = 0.1$; with this the reconstructions differences will be imperceptible. In fact, the optimal measurement points $\{t_k\}$ should be chosen to give approximately equal arc lengths of $u_r(1, \theta, t) = g(t)$. This will mean a far greater concentration of point for small values of t and this effect will be stronger the smaller the α value. We point out here that our time variable is actually a scaled version and physically incorporates a diffusion constant that can be quite small (for example, of the order of 10^{-5} for a metal). Thus the actual time measurements can be over the order of seconds or longer.

What if we delay the flux measurements until a later time, that is we measure only over $[T_0, T]$ for some $T_0 > 0$? There are certainly physical situations where this might be required. Note that Corollary 3.2 indicates uniqueness will still hold but the question is the resulting change in condition

17

number over incomplete intervals. Of course, the expected outcome is a decrease in the ability to construct higher modes as short-time information is lost. Further, when larger time values are missing the effect is greater for larger α and in particular, for the heat equation. This is again consistent with the above analysis.

In summary, the optimal time-measurement intervals for recovering the source support D in (1.1) depend strongly on α. Taking small initial time steps is advantageous in all cases but particularly important the smaller the value of α. If we are lacking such small-time measurements then or ability to reconstruct will be limited in any practical sense to a rough estimate of size and location with relatively little usable information for shape. Here the advantage shifts towards the fractional case as opposed to the heat equation.

4.6   More than two measurement points

We should expect superior reconstructions with a greater number of observation points since we have additional data for which to average out measurement error. However, (3.10) shows much more is possible since we see that if the difference $\theta_i - \theta_j$ is near to a rational number $\frac{p}{r}$ times π with some $r \leq M$, then the rth mode will be expressed very poorly from this combination. For a given M, the more observation points taken, the greater the opportunity to avoid this situation. This allows an often significant increase in the resulting singular values and correspondingly a better inversion of G' and hence of the reconstruction.

In experiment E_{2c}, we use four observation points.

$$q(\theta) = 0.5 + 0.05\cos\theta + 0.3\sin 2\theta,$$

$$E_{2c}: \quad \theta_1 = \frac{23}{32}\pi, \quad \theta_2 = \frac{57}{32}\pi, \quad \theta_3 = \frac{1}{4}\pi, \quad \theta_4 = \frac{39}{32}\pi,$$

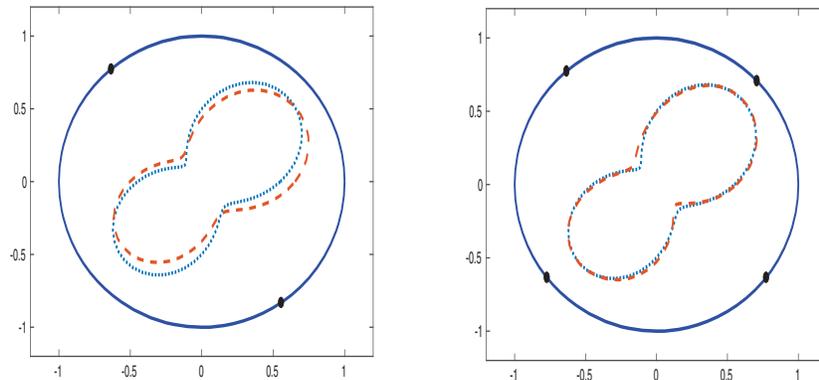$$\beta = 3 \times 10^{-2}, \ \delta = 1\%, \ \epsilon = \delta/10.$$

Figure 6: Results of experiments E_{2b} (left) and E_{2c} (right) with $\alpha = 0.9$.

The result is shown in Figure 6 and a vast improvement can be seen.

Acknowledgments

References

[1] Michele Caputo. Linear models of dissipation whose Q is almost frequency independent – II. *Geophys. J. Int.*, 13(5):529–539, 1967.

[2] Jin Cheng, Junichi Nakagawa, Masahiro Yamamoto, and Tomohiro Yamazaki. Uniqueness in an inverse problem for a one-dimensional fractional diffusion equation. *Inverse Problems*, 25(11):115002, 16, 2009.

[3] Mkhitar M Djrbashian. *Integral Transformations and Representation of Functions in a Complex Domain [in Russian]*. Nauka, Moscow, 1966.

[4] Mkhitar M. Djrbashian. *Harmonic Analysis and Boundary Value Problems in the Complex Domain*. Birkhäuser, Basel, 1993.

[5] Per Christian Hansen and Dianne Prost O'Leary. The use of the L-curve in the regularization of discrete ill-posed problems. *SIAM J. Sci. Comput.*, 14(6):1487–1503, 1993.

[6] F. Hettlich and W. Rundell. Identification of a discontinuous source in the heat equation. *Inverse Problems*, 17(5):1465–1482, 2001.

[7] Frank Hettlich and William Rundell. Iterative methods for the reconstruction of an inverse potential problem. *Inverse Problems*, 12(3):251–266, 1996.

[8] Bangti Jin, Raytcho Lazarov, and Zhi Zhou. An analysis of the L1 scheme for the subdiffusion equation with nonsmooth data. *IMA J. Numer. Anal.*, 36(1):197–221, 2016.

[9] Bangti Jin and William Rundell. An inverse Sturm-Liouville problem with a fractional derivative. *J. Comput. Phys.*, 231(14):4954–4966, 2012.

[10] Bangti Jin and William Rundell. A tutorial on inverse problems for anomalous diffusion processes. *Inverse Problems*, 31(3):035003, 40, 2015.

[11] Yikan Liu, William Rundell, and Masahiro Yamamoto. Strong maximum principle for fractional diffusion equations and an application to an inverse source problem. *Fract. Calc. Appl. Anal.*, 19(4):888–906, 2016.

[12] Francesco Mainardi, Antonio Mura, and Gianni Pagnini. The M-Wright function in time-fractional diffusion processes: a tutorial survey. *Int. J. Differ. Equ.*, pages Art. ID 104505, 29, 2010.

[13] Guofei Pang, Paris Perdikaris, Wei Cai, and George Em Karniadakis. Discovering variable fractional orders of advection-dispersion equations from field data using multi-fidelity Bayesian optimization. *J. Comput. Phys.*, 348:694–714, 2017.

[14] Kenichi Sakamoto and Masahiro Yamamoto. Initial value/boundary value problems for fractional diffusion-wave equations and applications to some inverse problems. *J. Math. Anal. Appl.*, 382(1):426–447, 2011.

[15] Stefan G. Samko, Anatoly A. Kilbas, and Oleg I. Marichev. *Fractional Integrals and Derivatives*. Gordon and Breach Science Publishers, Yverdon, 1993.

[16] Nicolás Garcí a Trillos and Daniel Sanz-Alonso. The Bayesian formulation and well-posedness of fractional elliptic inverse problems. *Inverse Problems*, 33(6):065006, 23, 2017.